COBEM 2025
28TH INTERNATIONAL CONGRESS OF MECHANICAL ENGINEERING

ABCM
Brazilian Society of Mechanical Sciences and Engineering
28th ABCM International Congress of Mechanical Engineering
November 09-14, 2025, Curitiba-PR, Brazil

COB-2025-0437
Effect of Weirs on Flow Control in Continuous Casting Tundishes

Ana Clara Santos Mauri
Andreza Thomaz Quaresma
Renato do Nascimento Siqueira
João Paulo Barbosa
IFES Campus São Mateus - Rodovia BR 101 north, km 58, Litorâneo, São Mateus - ES, 29932-540, Brasil
mauri09clara@gmail.com
andrezathomaz11@gmail.com
renatons@ifes.edu.br
jpbarbosa@ifes.edu.br

Abstract. *Metallurgical companies operating continuous casting processes rely on the tundish to ensure the quality of molten metal by promoting a uniform flow into the molds and reducing turbulence that may compromise steel purity. Flow control devices, such as weirs, dams, turbulence inhibitors, and gas curtains, are commonly employed to optimize tundish performance. However, the efficiency of these devices depends on their sizing and positioning, which must be evaluated to maximize productivity and final product quality. This study analyzed, based on numerical simulations using ANSYS Fluent R1 2025 with the k-epsilon turbulence model, the influence of weir positioning and height on the flow behavior within the tundish. The objective was to identify configurations that enhance flow stability and minimize recirculation zones, short-circuits and dead zones, contributing to improved flow control and reduced inclusions. To achieve this, CFD (Computational Fluid Dynamics) simulations were conducted, comparing two main conditions: a tundish without flow control devices and others containing weirs with different positions and heights. The results indicate that both the positioning and height of the weir directly influence the velocity fields and the presence of recirculation zones. Configurations with a weir positioned closer to the inlet and with moderate height favored a more stable flow, while others led to short-circuiting or stagnant regions. These findings reinforce the importance of evaluating geometric parameters when implementing flow control devices and provide guidance for improving casting performance, optimizing steelmaking operations, and reducing defects in the final product.*

Keywords: *Weir, Residence Time Distribution, Tundish, Computational Fluid Dynamics.*

1. INTRODUCTION

In the continuous steel casting process, the tundish serves as an intermediate vessel responsible for distributing molten steel to molds at a nearly constant rate. With the increasing demand for superior steel quality, its role has evolved from a simple distributor to a continuous-flow metallurgical reactor (Chen *et al.*, 2013).

To enhance fluid dynamics and promote inclusion removal, various Flow Control Devices (FCDs) are employed inside tundishes, including impact pads, dams, weirs, and perforated baffles. Among them, the weir plays a crucial role in redirecting molten steel upward, facilitating the flotation of non-metallic inclusions toward the slag layer (Jeon *et al.*, 2021). It also separates the inlet and pouring regions, helping to control turbulence and flow stratification (Chen *et al.*, 2013; Deng *et al.*, 2020).

Several studies have investigated tundish optimization using the weir in combination with other flow control devices. For example, Wang *et al.* (2020) employed a setup with a weir, turbulence inhibitor, and filter; Sheng and Chen (2021) analyzed a configuration with a weir, dam, gas curtain, and turbulence inhibitor; and Neves and Tavares (2017) studied the joint use of a weir, dam, turbulence inhibitor, and stop rod. While these combined approaches have demonstrated improvements in flow stability and inclusion removal, there is a notable lack of studies isolating the specific effect of the weir on tundish hydrodynamics. Such an approach is important for understanding its individual contribution and for optimizing its design without interference from other devices.

However, achieving optimal flow patterns remains a challenge. Non-ideal conditions, such as short-circuiting, dead zones, and recirculation regions, reduce the residence time and impair the tundish's refining capability. Teixeira and Siqueira (2008) define dead zones as stagnant regions with poor mass transfer; short-circuits as rapid-flow paths bypassing mixing; and recirculations as vortical structures that trap fluid in closed trajectories.

To quantify these phenomena, velocity fields and residence time distribution (RTD) curves are commonly analyzed. These tools help evaluate the effectiveness of FCD configurations in mitigating flow anomalies and enhancing steel cleanliness.

This study investigates the influence of the weir's geometric parameters, specifically its position and height, on the

internal hydrodynamics of a single-strand tundish. Six configurations are analyzed, including one without a weir. The results aim to identify arrangements that reduce dead volumes and recirculation while promoting a more uniform and controlled flow regime.

2. MATHEMATICAL MODELING

The mathematical modeling was based on a 3D standard set of the Navier–Stokes equations. The free surface is flat and is kept at a fixed level. The slag layer is not included.

The continuity equation for an incompressible flow is given by Eq. 1:

$$\frac{\partial \overline{U}_i}{\partial x_i} = 0 \tag{1}$$

where $\overline{U}_i$ is the mean velocity component in the i-direction. The Reynolds-averaged momentum equation, including the Boussinesq approximation for turbulence modeling, is described by Eq. 2:

$$\frac{\partial \overline{U}_i}{\partial t} + \overline{U}_j \frac{\partial \overline{U}_i}{\partial x_j} = -\frac{1}{\rho}\frac{\partial}{\partial x_i}\left(\overline{P} + \frac{2}{3}\rho k\right) + \frac{\partial}{\partial x_j}\left[(\nu + \nu_t)\left(\frac{\partial \overline{U}_i}{\partial x_j} + \frac{\partial \overline{U}_j}{\partial x_i}\right)\right] \tag{2}$$

$\overline{P}$ is the mean pressure, ρ is the fluid density, ν is the molecular kinematic viscosity, ν_t is the turbulent eddy viscosity, and k is the turbulent kinetic energy. The transport equation for the turbulent kinetic energy k is expressed in Eq. 3:

$$\frac{\partial k}{\partial t} + \overline{U}_j \frac{\partial k}{\partial x_j} = \frac{\partial}{\partial x_j}\left[\left(\nu + \frac{\nu_t}{\sigma_k}\right)\frac{\partial k}{\partial x_j}\right] + P - \varepsilon \tag{3}$$

The transport equation for the dissipation rate of turbulent kinetic energy ϵ is given by Eq. 4:

$$\frac{\partial \varepsilon}{\partial t} + \overline{U} j \frac{\partial \varepsilon}{\partial x_j} = \frac{\partial}{\partial x_j}\left[\left(\nu + \frac{\nu_t}{\sigma\varepsilon}\right)\frac{\partial \varepsilon}{\partial x_j}\right] + C_1 \frac{\varepsilon}{k} P - C_2 \frac{\varepsilon^2}{k} \tag{4}$$

In these equations, P denotes the production term of turbulent kinetic energy, while σ_k = 1.0 and σ_ϵ = 1.3 are the turbulent Prandtl numbers for k and ϵ, respectively. The constants C_1 = 1.44 and C_2 = 1.92 are empirical model coefficients. The turbulent kinematic viscosity ν_t used in the above equations is calculated using Eq. 5:

$$\nu_t = C_\mu \frac{k^2}{\varepsilon} \tag{5}$$

where C_μ =0.09 is a model constant. For scalar transport, such as mean concentration $\overline{C}$, the governing equation is provided by Eq. 6:

$$\frac{\partial \overline{C}}{\partial t} + \overline{U} j \frac{\partial \overline{C}}{\partial x_j} = \frac{\partial}{\partial x_j}\left[\left(D_m + \frac{\nu_t}{Sct}\right)\frac{\partial \overline{C}}{\partial x_j}\right] \tag{6}$$

D_m is the molecular diffusion coefficient and S_{ct} is the turbulent Schmidt number, assumed to be 0.7 in this study.

3. METHODOLOGY

The simulation of velocity fields and residence time distribution (RTD) curves was carried out using ANSYS Fluent R1 2025. Several hydraulic efficiency and mixing indicators can be calculated from the RTD curve to analyze flow quality. Siqueira (1998) recommended the use of the indicators t_i, t_{10}, Mo and σ^2.

The geometry and simulation conditions were adopted from Sheng and Jonsson (2021). Figure 1 presents the geometry. Symmetry was applied to reduce the computational cost.

The distance between the beginning of the tundish and the inlet is 0.576 m, while the distance between the end of the tundish and the outlet is 0.412 m. The diameters of the inlet and outlet are 0.06 m. The width of the weir is 0.056 m. The surface wall was defined as free slip, whereas the remaining walls were defined as no slip.

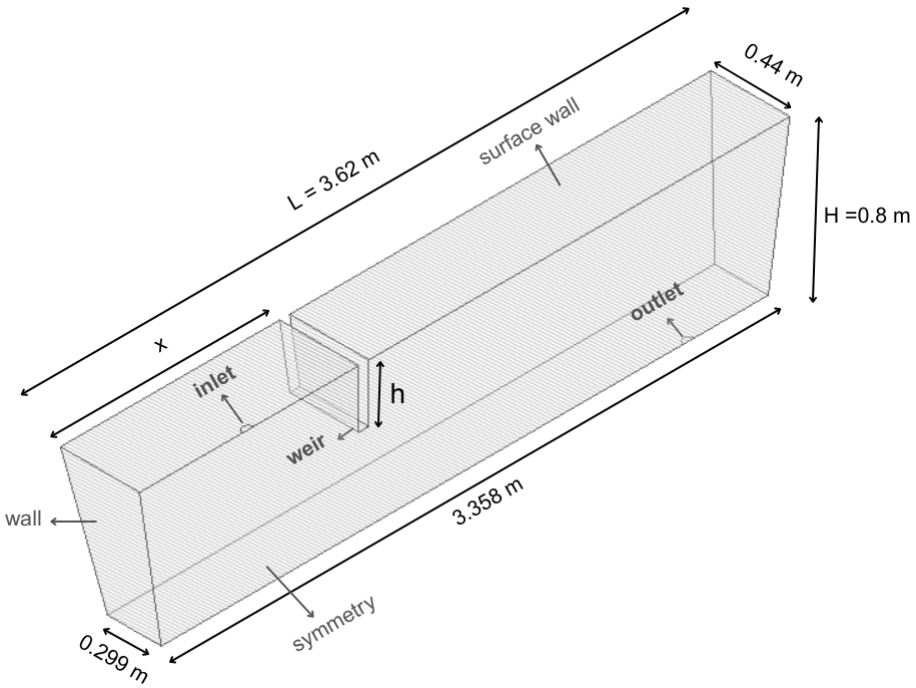

Figure 1. Three-dimensional geometry of a single-strand tundish with a weir, showing its main dimensions and boundary regions: inlet, outlet, wall, symmetry plane, and surface.

Six different geometries were simulated based on Fig. 1, by varying the values of h/H and x/L, thereby modifying both the position and height of the weir three times each. The selected values for weir height and position were based on the study by de Almeida (1997). One of the geometries did not include a weir, allowing for an assessment of its influence on the tundish flow. Table 1 presents the values of x/L and h/H used to vary the weir's position and height.

Table 1. Positions and relative height of the weirs used for the simulations

Values of x/L			**Values of h/H**		
$\mathbf{x_1/L}$	$\mathbf{x_2/L}$	$\mathbf{x_3/L}$	$\mathbf{h_1/H}$	$\mathbf{h_2/H}$	$\mathbf{h_3/H}$
0.225	0.337	0.450	0.200	0.400	0.600

First, the tundish without the weir was simulated. Then, using the average height h_2, three cases were simulated by varying the positions x_1, x_2, and x_3. After selecting the best position among the three, two additional cases were simulated by varying the height to h_1 and h_3.

The simulation was performed using water as the working fluid. The realizable $k-\epsilon$ turbulence model was adopted due to its lower computational cost and suitability for flows where fine resolution of the boundary layer is not essential. For the numerical solution, the SIMPLE algorithm was applied in the steady-state analysis, as it is preferred for stationary scenarios due to its efficiency and simplicity, while the Coupled algorithm was used in the transient simulations for its superior coupling between variables and greater robustness in handling time advancement. The inlet velocity was set to 0.236 m/s. A second-order upwind scheme was employed to discretize the convective fluxes in the momentum equations, ensuring improved accuracy in capturing flow gradients. The under-relaxation factors for the flow calculations were set to 0.3 for pressure, 0.7 for velocity, and 0.8 for turbulence parameters.

Considering the inlet velocity of 0.236 m/s, the inlet diameter of 0.06 m, and the physical properties of water at room temperature ($\rho = 998.2\ kg/m^3$, $\mu = 1.002 \times 10^{-3}\ Pas$), the Reynolds number was estimated at approximately 1.41×10^4. This value characterizes the flow as fully turbulent, reinforcing the appropriateness of the selected turbulence model. This also confirms the applicability of CFD models for analyzing turbulent regimes in tundishes.

4. RESULTS AND DISCUSSIONS

4.1 Mesh Independence Test

For the mesh independence test, five prismatic meshes with different element sizes were used in a bare tundish, as shown in Tab. 2.

Table 2. Mesh characteristics used in the mesh independence test, with different sizes, nodes, and elements.

Mesh	Element size (m)	Nodes	Elements
Mesh 1	0.100	3,629	17,145
Mesh 2	0.075	5,854	28,232
Mesh 3	0.060	9,389	47,184
Mesh 4	0.050	14,888	76,570
Mesh 5	0.040	27,362	143,974

Figure 2 shows the residence time distribution (RTD) curves corresponding to the meshes described in Table 2. The meshes 1 and 2, with element sizes of 0.1 m and 0.075 m, had lower computational costs but showed more pronounced differences in the solution profile, especially in the peak region. Starting from the mesh 3, the behavior among the meshes became visually similar.

According to Siqueira (1998), σ^2 (the dispersion index) is the most physically meaningful mixing indicator, as it is directly related to the variance of the RTD curve. Compared to the most refined mesh, the coarser meshes (1 and 2) exhibited a dispersion index difference of over 9%. In contrast, the meshes 3 and 4 showed variations of less than 2%. Therefore, due to its lower computational cost and sufficient accuracy, the mesh with an element size of 0.06 m was selected for this study.

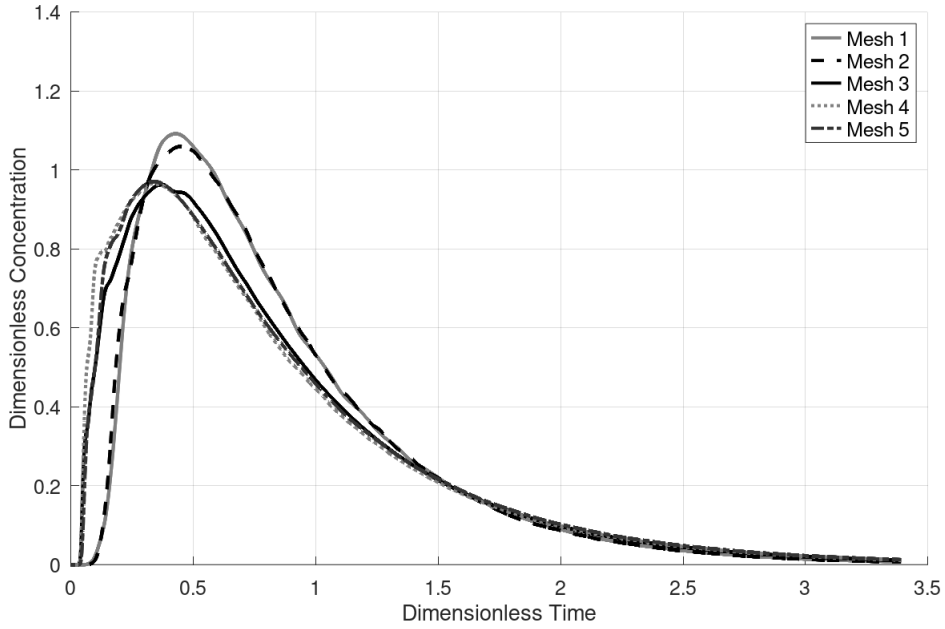

Figure 2. RTD curves of the bare tundish for five mesh configurations from the mesh independence test.

4.2 Model Validation

The CFD model was validated by comparing its results with the water model experiments reported by Chen *et al.* (2013), which evaluated residence time distribution (RTD) curves in a single-strand bare tundish under geometrical and dynamic similarity criteria. Figure 3 shows the comparison between the RTD curve obtained from the present numerical simulation and the experimental results from Chen *et al.* (2013). The overall shape and trend of both curves are consistent, showing a rapid rise, a distinct peak, and a gradual decay. The peak concentration and breakthrough time are very similar between the two curves, with only minor deviations in the tailing region. The similarity in the ascending and descending slopes indicates that the CFD model was able to reproduce the main hydrodynamic behavior of the flow within the tundish.

These results suggest that the numerical model captures the essential features of the residence time distribution and is suitable for analyzing the flow behavior and evaluating the influence of flow control devices such as weirs.

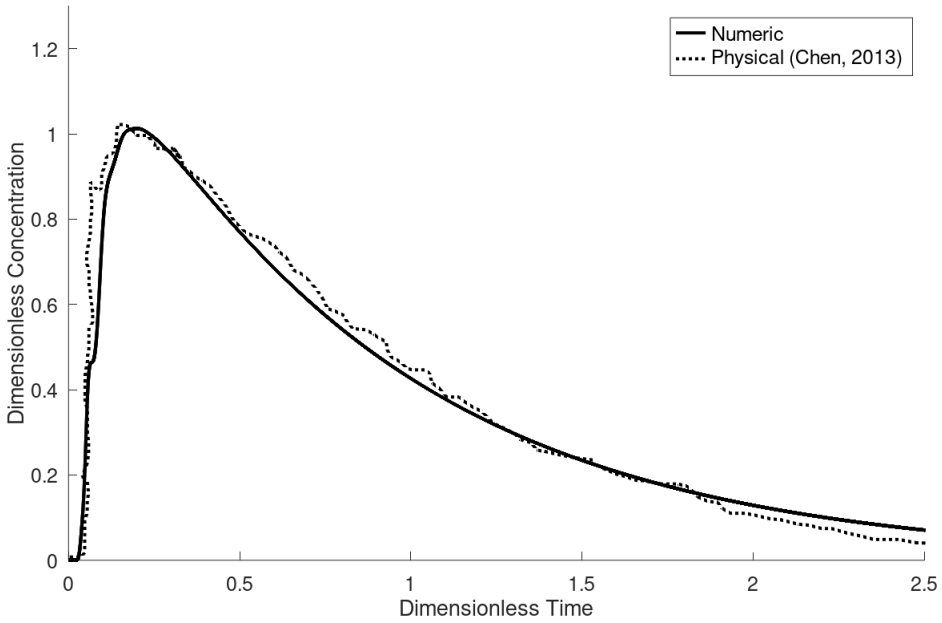

Figure 3. Comparison of the simulated Bare Tundish curve with the results from Chen (2013)

4.3 Effects of Weir Position and Height on Flow Dynamics

Figure 4 shows the velocity field vectors for the bare tundish and for the tundishes with the weir positioned at different locations. It can be visually observed that the bare tundish exhibits recirculation zones on the left side, which are also present in the other geometries.

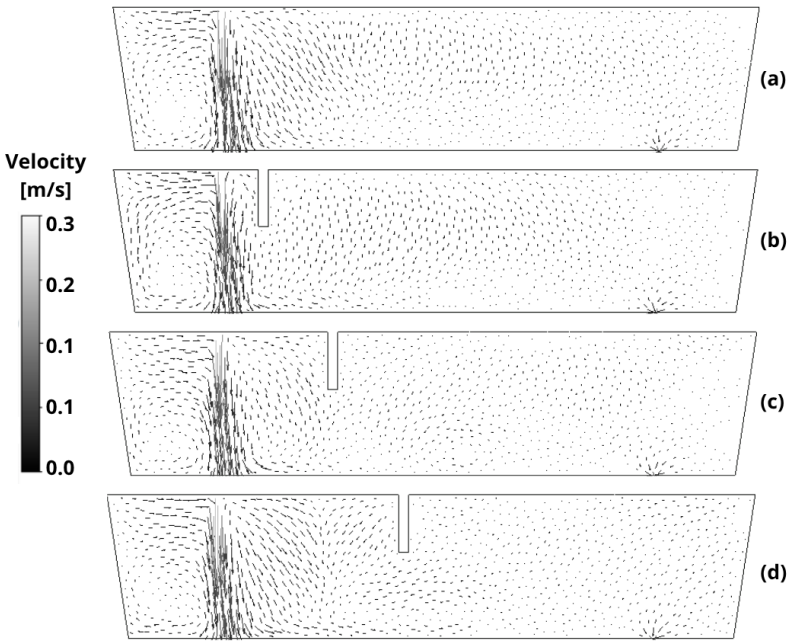

Figure 4. Velocity field vectors. (a) Bare tundish; (b) Tundish with position x_1 and height h_2; (c) Tundish with position x_2 and height h_2; (d) Tundish with position x_3 and height h_2.

Figure 5 presents the RTD curves for tundishes with weirs positioned at x_1, x_2, and x_3, all with the same relative height h_2, in comparison to the bare tundish. The curve corresponding to position x_2 closely resembles the bare tundish, suggesting that this weir placement had a limited impact on the flow pattern. In contrast, the configuration with position x_3 led to an earlier and more pronounced peak, indicating the formation of short-circuiting, where part of the fluid reaches

the outlet faster, reducing residence time and potentially affecting inclusion removal. The configuration with the weir at position x_1 showed the highest and narrowest peak among all cases, deviating significantly from the others. These results demonstrate that placing the weir closer to the inlet (as in x_1) can disrupt the flow path more aggressively, while intermediate positioning (x_2) might not alter the flow sufficiently.

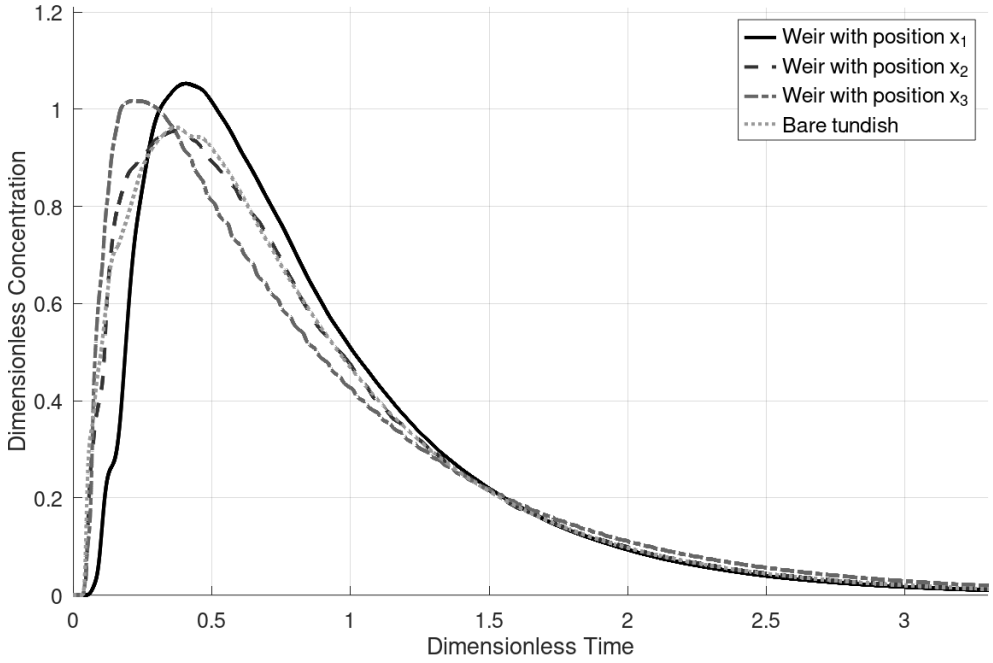

Figure 5. RTD curves for different weir positions compared to the bare tundish

Table 3 presents the calculation of the indicators for each residence time distribution curve. t_i is the initial time at which the tracer begins to exit the unit, while t_{10} represents the time required for 10% of the tracer mass to leave the unit (Teixeira and Siqueira, 2008). Both indicators are useful for identifying the intensity of short-circuiting phenomena. The Morril Index (Mo) is the ratio between the times at which 90% and 10% of the tracer mass has exited the unit, and its value is influenced by the presence of dead zones. The dispersion index σ^2 accounts for the entire residence time curve and is calculated as described by Siqueira (1998). This indicator is also useful for evaluating the degree of mixing within the unit.

Table 3. Indicators corresponding to changes in the weir position

Indicators	t_i	t_{10}	Mo	σ^2
Bare tundish	0.036	0.213	7.72	1.538
Weir with position x_1 and height h_2	0.061	0.283	5.72	1.449
Weir with position x_2 and height h_2	0.039	0.214	7.75	1.539
Weir with position x_3 and height h_2	0.037	0.189	9.35	1.619

Regarding the indicators t_i and t_{10}, all weir configurations increased the initial tracer response time compared to the bare tundish, suggesting a reduction in short-circuiting. The configuration with the weir at position x_1 yielded the highest t_i and t_{10}, indicating the most effective delay in tracer breakthrough. However, its lower Morril index Mo implies a narrower RTD curve, which may reflect a more plug-like flow but also a potential reduction in mixing. In contrast, the weir at position x_3 exhibited the highest Mo and σ^2, suggesting enhanced mixing but also the possibility of more dispersed flow and dead zones. Only the configuration with x_1 resulted in a lower σ^2 than the bare tundish, reinforcing its role in stabilizing the flow and minimizing dispersion. These results demonstrate that although all weir positions contributed to mitigating short-circuiting, their effects on flow uniformity and mixing varied notably depending on the location.

Overall, the weir at position x_2 exhibited indicator values very similar to those of the bare tundish. The weir at position x_3, however, showed a deterioration in all indicators compared to the bare tundish. In contrast, the weir placed at x_1, closest to the inlet, resulted in improvements across all indicators.

Since the position x_1 yielded the best results among the studied configurations, additional analyses were conducted on

the tundish with a weir placed at this position, considering different weir heights: h_1 and h_3, in addition to the previously studied h_2. The velocity vector fields for these cases, as well as for the bare tundish, are shown in Fig. 6.

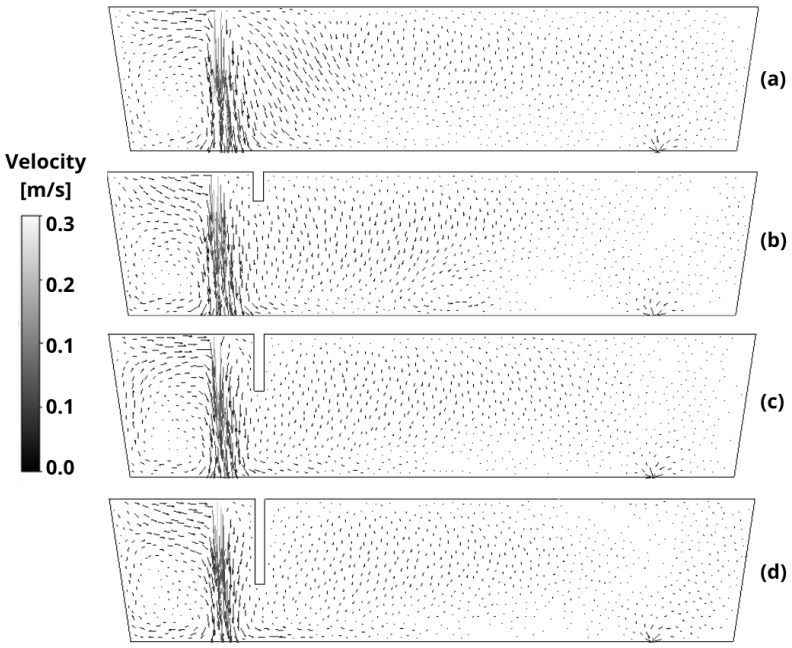

Figure 6. Velocity field vectors. (a) Bare tundish; (b) Tundish with position x_1 and height h_1; (c) Tundish with position x_1 and height h_2; (d) Tundish with position x_1 and height h_3.

Figure 7 shows the residence time distribution curves for the different weir heights used at position x_1. The behavior of the curves is more similar compared to the variations observed when analyzing different weir positions. As seen in Fig. 6, the velocity vectors also followed similar paths, with only slight differences in the dead zones. The RTD curves show minimal variation between the different weir heights, and no significant differences can be observed in the flow behavior.

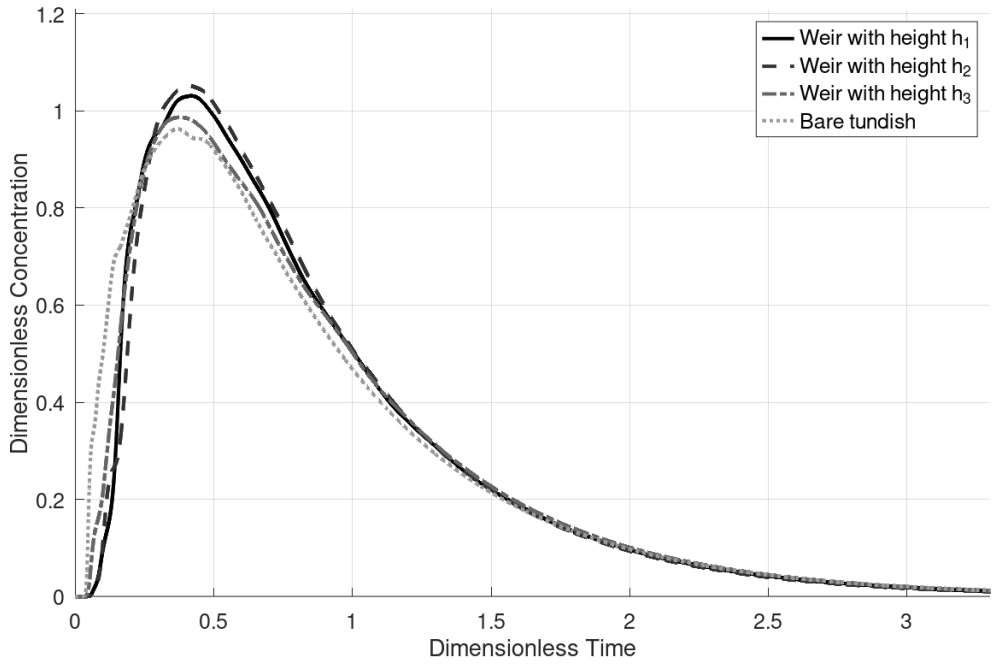

Figure 7. RTD curves for different weir heights compared to the bare tundish

Table 4 presents the values of the performance indicators calculated for each weir height configuration, in comparison with the bare tundish. All configurations with a weir showed improved results compared to the bare tundish. Among the studied cases, the configuration with the weir at position x_1 and height h_2 achieved the best performance, with the highest values of t_i and t_{10}, and the lowest values of Mo and σ^2.

Table 4. Indicators corresponding to changes in the weir height

Indicators	t_i	t_{10}	Mo	σ^2
Bare tundish	0.036	0.213	7.72	1.538
Weir with position x_1 and height h_1	0.058	0.269	6.08	1.466
Weir with position x_1 and height h_2	0.061	0.283	5.72	1.449
Weir with position x_1 and height h_3	0.043	0.255	6.54	1.486

Based on the analysis of weir positions and heights in the tundish, including velocity field vectors, residence time distribution curves, and performance indicators, the configuration with the weir at position x_1 and height h_2 showed slightly better results. However, the differences between the cases were small, suggesting that the influence of weir position and height on overall tundish performance was limited under the conditions studied.

5. CONCLUSIONS

The results indicate that both the position and height of the weir influence the velocity fields and the development of short-circuit paths, dead zones, and recirculation regions. A weir positioned closer to the fluid inlet tended to redirect the flow more effectively, potentially reducing short-circuiting and enhancing flow uniformity. Regarding height, the configuration with a height-to-total ratio of 0.4 showed slightly better performance than those with lower or higher weirs. This may indicate that excessively tall weirs do not significantly improve flow redirection, while shorter weirs might even hinder it. Although the differences between configurations were relatively small, the results suggest the existence of an optimal range for both weir position and height that could promote more favorable hydrodynamic conditions compared to the bare tundish.

6. ACKNOWLEDGEMENTS

This work was carried out with support from the Espírito Santo Research and Innovation Support Foundation (FAPES - Fundação de Amparo à Pesquisa e Inovação do Espírito Santo) – T.O. 1052/2022. The authors also thank FAPES for the grant funding that enabled this study to be conducted.

7. REFERENCES

Chen, D., Xie, X., Long, M., Zhang, M. and Liao, Q., 2013. "Hydraulics and mathematics simulation on the weir and gas curtain in tundish of ultratick slab continuous casting". *Metallurgical and Materials Transactions*, Vol. 45B, pp. 392–398.

de Almeida, M.M.P., 1997. *Estudo do efeito de defletor de escoamento e da relação comprimento/largura efetiva do escoamento na eficiência hidráulica de bacia de sedimentação*. Master's thesis, Graduate Program in Ambiental Engineering, Federal University of Espírito Santo, Espírito Santo, Brasil.

Deng, X., Liu, G., Qiangqiang, W., Liu, B., Ji, C., Li, H. and Shao, X., 2020. "Effect of the weir structure in the tundish on the cleanliness of if steels and elimination of spot-like defects in deep drawing automobile steel sheets". *Metallurgical Research Technology*, Vol. 117.

Jeon, S., Lee, S., Ha, S., Kim, S. and You, D., 2021. "Effects of a moving weir on tundish flow during continuous-casting grade-transition". *Journal of Mechanical Science and Technology*, Vol. 35, No. 9, pp. 4001–4009.

Neves, L. and Tavares, R.P., 2017. "Analysis of the mathematical model of the gas bubbling curtain injection on the bottom and the walls of a continuous casting tundish." *Ironmak*, Vol. 44, pp. 559–567.

Sheng, D.Y. and Chen, D., 2021. "Comparison of fluid flow and temperature distribution in a single-strand tundish with different flow control devices". *Metals 2021*, Vol. 11, No. 796.

Sheng, D.Y. and Jonsson, P.G., 2021. "Effect of thermal buoyancy on fluid flow and residence-time distribution in a single-strand tundish". *Materials 2021*, Vol. 14.

Siqueira, R.N., 1998. *Desenvolvimento e Aperfeiçoamento de Critérios de Avaliação da Eficiência Hidráulica e do Cálculo do Coeficiente de Mistura em Unidades de Tratamento de Água e Efluentes*. Master's thesis, Graduate Program in Ambiental Engineering, Federal University of Espírito Santo, Espírito Santo, Brasil.

Teixeira, E.C. and Siqueira, R.N., 2008. "Perfomance assesment of hydraulic efficiency indexes". *Journal of Environmental Engineering*, Vol. 134, p. 851.

Wang, Q., Liu, Y., Huang, A., Yan, W., Gu, H. and Li, G., 2020. "Cfd investigation of effect of multi-hole ceramic filter on inclusion removal in a two-strand tundish". *Metallurgical and Materials Transactions*, Vol. 51B, pp. 276–292.

8. RESPONSIBILITY NOTICE

The authors are solely responsible for the printed material included in this paper.